Wavefield characterization of nearly diffraction-limited focused hard x-ray beam with size less than 10 nm

Takashi Kimura,[1,a)] Hidekazu Mimura,[1] Soichiro Handa,[1] Hirokatsu Yumoto,[2] Hikaru Yokoyama,[1] Shota Imai,[1] Satoshi Matsuyama,[1] Yasuhisa Sano,[1] Kenji Tamasaku,[3] Yoshiki Komura,[3] Yoshinori Nishino,[4] Makina Yabashi,[2] Tetsuya Ishikawa,[2,3] and Kazuto Yamauchi[1,5]

[1]*Department of Precision Science and Technology, Graduate School of Engineering, Osaka University, 2-1 Yamada-oka, Suita, Osaka 565-0871, Japan*
[2]*SPring-8/Japan Synchrotron Radiation Research Institute (JASRI), 1-1-1 Kouto, Sayo, Hyogo 679-5198, Japan*
[3]*SPring-8/RIKEN, 1-1-1 Kouto, Sayo, Hyogo 679-5198, Japan*
[4]*Research Institute for Electric Science, Hokkaido University, Kita 21 Nishi 10, Kita-ku, Sapporo 001-0021, Japan*
[5]*Center for Ultra-Precision Science and Technology, Graduate School of Engineering, Osaka University, 2-1 Yamada-oka, Suita, Osaka 565-0871, Japan*

(Received 5 August 2010; accepted 8 October 2010; published online 29 December 2010)

In situ wavefront compensation is a promising method to realize a focus size of only a few nanometers for x-ray beams. However, precise compensation requires evaluation of the wavefront with an accuracy much shorter than the wavelength. Here, we characterized a one-dimensionally focused beam with a width of 7 nm at 20 keV using a multilayer mirror. We demonstrate that the wavefront can be determined precisely from multiple intensity profiles measured around the beamwaist. We compare the phase profiles recovered from intensity profiles measured under the same mirror condition but with three different aperture sizes and find that the accuracy of phase retrieval is as small as λ/12. [doi:10.1063/1.3509384]

I. INTRODUCTION

A coherent and monochromatic electromagnetic wavefield is characterized by amplitude and phase. Although the intensity distribution, which is equivalent to the square of the amplitude, can be detected, the phase distribution of the wavefield is not directly measurable by any method. For this reason, various methods of wavefront determination using intensity information, such as interferometry based on phase shifting,[1–3] holography with a reference beam,[4,5] and phase retrieval with iterative calculation,[6,7] have been developed in the past. One of the purposes of wavefront measurement is for the compensation of an aberration in an imaging optical system.[8–10] *In situ* wavefront correction has the potential to realize diffraction-limited resolution imaging, even if the performances of focusing or imaging optical devices, such as lenses and mirrors, are insufficient.

In particular, wavefront correction is an effective technique for a hard x-ray focusing system, because the hard x-ray focusing device requires an unprecedented accuracy of fabrication to achieve its theoretical performance.[11] The construction of any interferometric optical system is relatively difficult from the viewpoint of producing detectable interference fringes with extremely short wavelength light. On the other hand, in an x-ray imaging field, coherent diffractive imaging using iterative calculation is now considered to be promising for achieving nanometer spatial resolution.[12–14] In these methods, by using the x-ray diffraction pattern originating from a sample, both the wavefield distribution at a sample and that at a camera position are reconstructed by iterative calculation.

The concepts of wavefield reconstruction in coherent diffractive imaging are applicable to the wavefront measurement in a hard x-ray focusing system. By phase retrieval calculation using only intensity profiles around the focal point, the determination of wavefields on a focusing device and on a focused x-ray beam is possible. The *in situ* wavefront correction system consisting of wavefront control and measurement has already been proposed and successfully applied to a sub-10-nm hard x-ray focusing system[15,16] with a newly developed beam intensity profile measurement method.[17]

In this study, in order to improve the accuracy of the wavefront correction system for hard x-ray focusing and extend the range of application of the wavefront measurement, we characterized a focused hard x-ray 7-nm beam and investigated the degree of accuracy in recovered wavefront error profiles. We performed an x-ray focusing test with a 20-mm-long multilayer mirror and recovered three wavefront errors using three different experimentally measured beamwaist structures obtained by changing the entrance aperture size. Comparing the independently reconstructed wavefront error profiles, we clarified the degree of wavefront error of the focused x-ray beam with an accuracy better than λ/12, which corresponds to a height of 0.38 nm on the surface of the focusing mirror, and confirmed that the achieved spot size nearly reached to the diffraction limit of 7 nm.

II. PHASE RETRIEVAL USING THE INTENSITY PROFILES OF FOCUSED BEAM

A. Algorithm

Following Fraunhofer diffraction theory, the relation between the complex wavefield at the entrance pupil and at the

a)Electronic mail: kimura@up.prec.eng.osaka-u.ac.jp.

focal plane is expressed by a Fourier transform and an inverse Fourier transform. In an x-ray focusing system using mirror optics, the intensity distribution at the entrance pupil is ideal. On the other hand, the phase distribution is distorted due to the misalignment, figure errors, and imperfections in the multilayer structures. To characterize this phase distribution of focused beam, several wavefield reconstruction techniques of focused x-ray beam from far-field diffraction pattern have been proposed and demonstrated.[18–20] According to the Fourier transform relationship, long-spatial-frequency components of phase distortion at the entrance pupil, namely aberration, strongly affect the shape of intensity profiles near the focus. In other words, a phase retrieval method that utilizes intensity profiles near focus is sensitive to long-spatial-frequency components of phase information at the entrance pupil; such a method is adequate for a wavefront correction system. However, in hard x-ray regions, it is difficult to measure the intensity profile of a focused beam. The measured intensity profiles include measurement errors, which lead to an invalid solution in phase retrieval.

In this study, we employed an advanced phase retrieval algorithm using a nonlinear optimization approach.[21] In this method, many intensity profiles around the focal point are inputted into iterative calculations. The nonlinear optimization calculation is employed for the convergence acceleration. The phase information near the focus and on the entrance pupil are outputted when the square error between measured and reconstructed intensity profiles is minimized.

The schematic of the optical system used for phase retrieval is shown in Fig. 1. Initially, N planes are set around the focal point. $I_j(r)$ and $E_j(r)$ are the measured intensity profiles and the assumed wavefield of the jth plane, respectively. $E_i\langle E_j(r)\rangle$ is the wavefield of the ith plane derived from that of the jth plane, which is calculated using the angular spectrum method.[22]

To evaluate the assumed wavefield $E_j(r)$, the error function is set to be the sum of squared errors of the intensity profiles as

$$\mathrm{Error}_j = \sum_{i\neq j}\sum_{r}\left[\sqrt{I_i(r)} - |E_i\langle E_j(r)\rangle|\right]^2. \tag{1}$$

The gradient of the error function with respect to $\theta_j(r)$ is simply expressed as

$$\frac{\partial \mathrm{Error}_j}{\partial \theta_j(r)} = 2\ \mathrm{Im}\left[E_j(r)\sum_{i\neq j}E_j^*\left\langle\sqrt{I_i(r)}\frac{E_i\langle E_j(r)\rangle}{|E_i\langle E_j(r)\rangle|} - E_i\langle E_j(r)\rangle\right\rangle\right]. \tag{2}$$

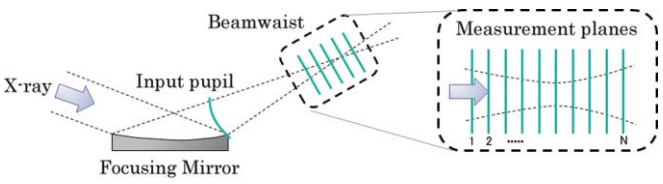

FIG. 1. (Color online) Schematic of optical system for phase retrieval.

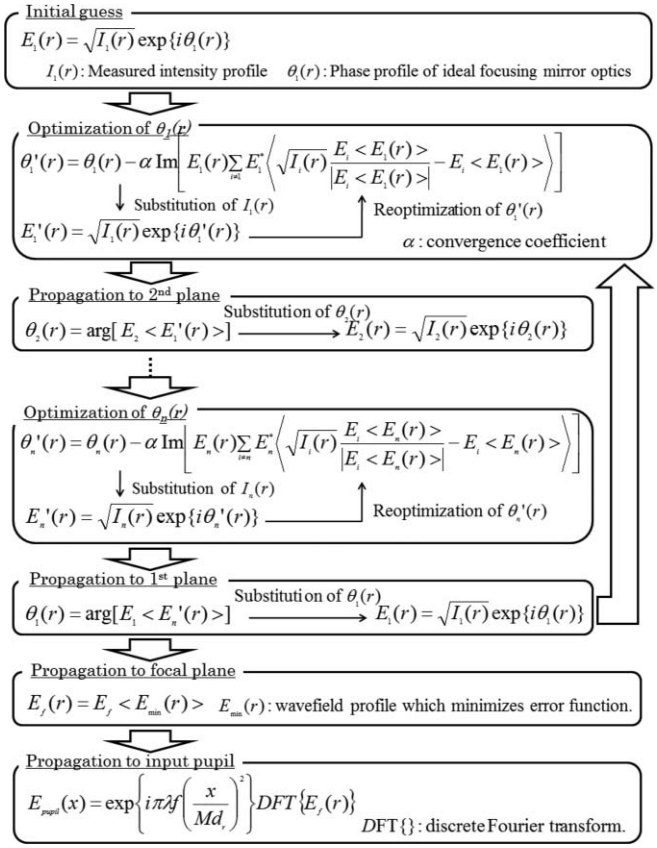

FIG. 2. Block diagram of phase retrieval algorithm.

In Eq. (2), $\theta_j(r)$ is the phase component of $E_j(r)$, which is written as

$$E_j(r) = |E_j(r)|\exp\{i\theta_j(r)\}. \tag{3}$$

Using Eq. (2), the optimized $\theta_j(r)$ of the jth plane is calculated, so that the error function is minimized.

Figure 2 shows the details of the optimization procedure. The initial wavefield $E_1(r)$ consists of the measured intensity profile $I_1(r)$ and the ideal phase profile $\theta_1(r)$. $\theta_1(r)$ is processed in the nonlinear optimization using Eq. (2). $\theta_1(r)$ is increased or decreased in each iteration to reduce the value of Eq. (1). When the value of Eq. (1) is small enough, the iterative calculation is stopped.

In the next step, the main plane where the phase is optimized is shifted to another plane. The initial wavefield $E_2\ \langle E_1'(r)\rangle$ is calculated by the angular spectrum method using only $E_1'(r)$. The amplitude of $E_2\langle E_1'(r)\rangle$ is changed to the measured one. Then, only the phase profile on this plane is optimized by the method described above.

The shift of the main plane and the optimizations of phase profiles are repeated until the value of the error function in Eq. (1) becomes sufficiently small. The final wavefield $E_f(r)$ of the focal plane is propagated to the input pupil in accordance with Fraunhofer diffraction theory

$$E_{\mathrm{pupil}}(x) = \exp\left\{\frac{i\pi}{\lambda f}(d_x x)^2\right\}\mathrm{DFT}\{E_f(r)\}, \tag{4}$$

where f is the focal length of the focusing mirror and d_x is the pixel size in the input pupil, which is given by

TABLE I. Optical parameters of wave-optical simulation of system.

Mirror length (mm)	20
Glancing angle (mrad)	7.0
Focal length (mm)	20

$$d_x = \frac{\lambda f}{M d_r}. \quad (5)$$

Here, M and d_r are the array size and scanning pitch of the measured profiles, respectively.

B. Simulation results

Table I and Fig. 3 show the simulated optical parameters and the wavefront error on the mirror surface in the demonstrations, respectively. The focused beam has a full width at half maximum (FWHM) of 7 nm. Figure 4(a) shows the inputted data of the beamwaist structure obtained using a wave-optical simulator coded on the basis of the Fresnel–Kirchhoff diffraction integral theory.[23] The data consisted of 21 measured planes. The interval between each plane was 2 μm. Approximately 2500 iteration calculations (see Fig. 2) were performed to obtain the optimized phase distribution. The recovered intensity distribution obtained by the phase retrieval calculation is shown in Fig. 4(b). The recovered profile was in good agreement with the assumed profile.

Figure 5 shows the derived wavefield distribution at the input pupil located 8 mm upstream of the focal plane. The complex amplitude of the incident beam is larger than zero within only the aperture area, which is equal to the assumed size. The wavefront error profiles are also similar. The difference between the two profiles was 0.029 rad root mean square (rms).

III. EXPERIMENT

The experiment for measuring the wavefront error of a multilayer mirror was performed at the 1-km-long beamline of SPring-8.[24] A schematic drawing of the experimental setup is shown in Fig. 6. The focusing mirror was a laterally graded Pt/C multilayer optic[16] with a theoretical FWHM spot size of 7 nm at an x-ray energy of 20 keV. The spatial coherence of the incident x-ray beam was sufficiently high for this experiment. [25]

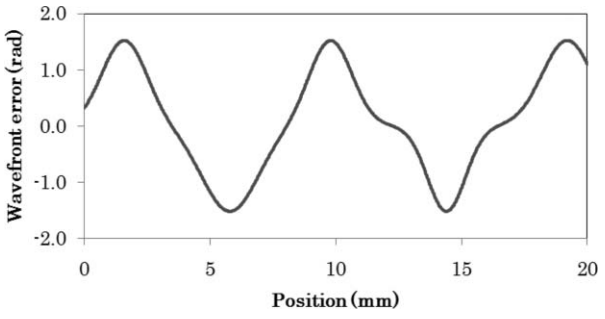

FIG. 3. Wavefront error profile assumed on focusing mirror surface. The peak-to-valley wavefront error height corresponds to 1/2λ.

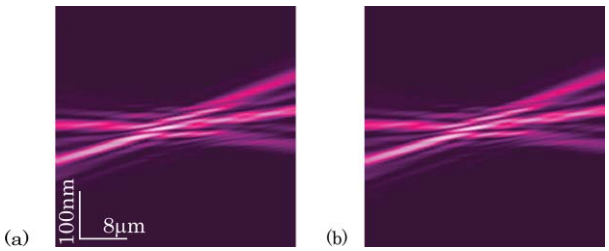

FIG. 4. (Color online) Comparison between original and recovered beamwaist structures in phase retrieval calculation. (a) Original beamwaist. (b) Recovered beamwaist.

Conventional knife-edge scan method becomes difficult, when the depth of the focus decreases shorter than the attenuation length of the edge material. In the focused beam profile measurement, the dark-field knife-edge scan method[17] using a phase object of platinum was employed. The focal depth of the 7 nm beam is approximately 5 μm. Thus, the phase object, which was 1 μm wide in the beam direction, was fabricated using a focused ion-beam fabrication system (HITACHI FB-2100). The surface roughness of the phase object was directly measured with an atomic force microscope (Shimadzu SFT-3500 SPM) and it was confirmed to have a flatness of rms 1.06 nm.

Figures 7(a)–7(c), respectively, show the beamwaist structures measured when the aperture size of the focusing mirror was the full size and restricted to two-thirds and one-third of its size by the slit just upstream of the focusing mirror. Each beamwaist structure obtained from 16 intensity profiles. The interval of the profiles in the direction of the optical axis was 2 μm. When the aperture was fully open, the minimum focused spot has an FWHM of 7 nm.

Figures 7(d)–7(f) show the beamwaist structures reconstructed from the measured beamwaist structures in Figs. 7(a)–7(c), respectively. They agree well with the experimental results, indicating the reliability of the phase retrieval calculation. The recovered amplitudes at the input pupil located 8 mm upstream of the focal plane obtained by utilizing each reconstructed beamwaist structure are shown in Fig. 8(a). The size of the recovered input pupil increased proportionally with the aperture size. In the case of a fully open aperture, the size of the recovered input pupil was approximately 70 μm, which is equal to the ideal value. The calculated wavefront errors extracted from the recovered aperture areas are shown in Fig. 8(b). The final wavefront error

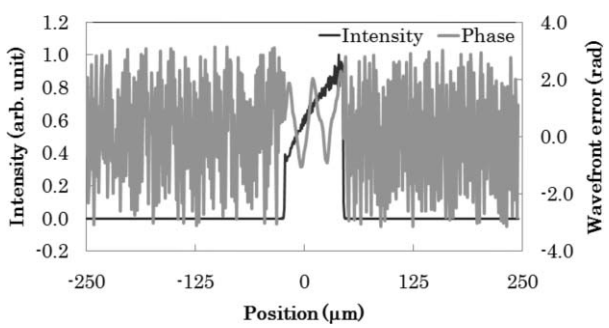

FIG. 5. Results of numerical simulation of phase retrieval calculation.

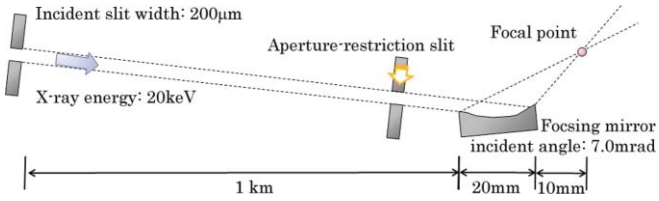

FIG. 6. (Color online) Schematic of experimental setup.

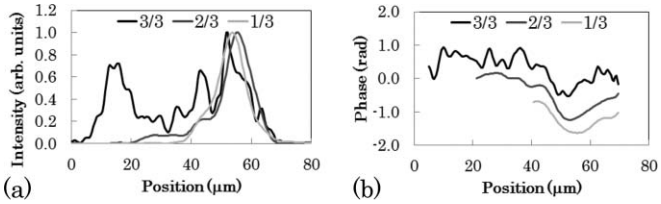

FIG. 8. Comparison of experimental results of phase retrieval calculations. (a) and (b) The recovered intensity and wavefront error profiles at the input pupil, respectively.

profiles in the superposition area show good agreement with each other. The difference in wavefront error between the three recovered profiles and their average was 0.54 rad peak-to-valley (P–V).

IV. DISCUSSION

Figure 7(g) shows the beamwaist profile derived from the input pupil wavefield calculated using the recovered phase profile in Fig. 8(b) and the ideal intensity profile of the focusing mirror. The two beamwaist profiles in Figs. 7(d) and 7(g) show good agreement even when the intensity profiles on the input pupil are different. This result indicates that the recovered intensity profile of the input pupil is more sensitive than the phase profile to measurement noise.[21,26] In this study, we applied the algorithm that optimizes only the measured beamwaist profiles using the evaluation function of Eq. (1). Measurement errors that result from vibration and the imperfection of the phase object directly affect the recovered wavefield of the input pupil. These effects tend to appear in the measurement of small focused beam with large numerical aperture. In particular, such effects appear in the values of the recovered amplitude.

However, compared with the intensity profile of the input pupil, the phase profile of the input pupil should be well defined. When the numerical aperture is changed, the fringe patterns observed in the beamwaist structure are markedly different. The recovered wavefront errors derived from these beamwaist structures are also entirely independent of each other. The phase profiles of the common area should be the same. Although the recovered phase profile in the case of the fully open aperture seems to be slightly noisy because of the measurement errors, the agreement within 0.54 rad P–V indicates the reliability of the recovered phase information in the developed method.

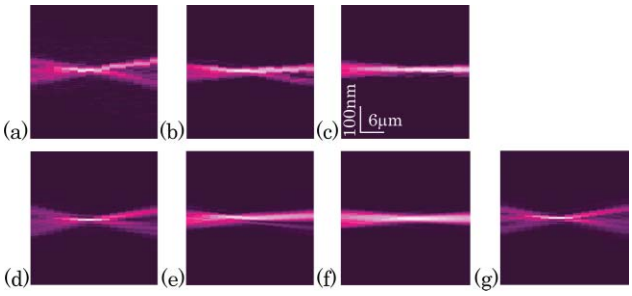

FIG. 7. (Color online) Measured and reconstructed intensity profiles near focal point. (a)–(c) The beamwaist structures measured under the following conditions: the aperture size of the focusing mirror was restricted to full size, $\frac{2}{3}$ and $\frac{1}{3}$ by the slit slightly upstream of the focusing mirror. (d)–(f) The beamwaist structures reconstructed from (a)–(c). (g) The beamwaist profile derived from the input pupil wavefield calculated using the recovered phase profile in Fig. 8(a) and the ideal intensity profile of the focusing mirror.

When the aperture of the mirror was fully open, the calculated wavefront error was only approximately 0.23λ P–V. This corresponds to a figure error height of 1.0 nm at the mirror surface. For this reason, the achieved spot size nearly reached the diffraction limit of 7 nm. In contrast to our previous report,[16] we successfully focused an x-ray beam to a sub-10-nm spot size without employing an adaptive mirror. In this case, both the mirror length and the focal length are shorter than those in the previous case. Owing to the easier alignment than in the previous optical system, a nearly diffraction-limited focusing state was possible without phase compensation.

In this study, we have developed a wavefront error metrology using intensity profiles near the focus in hard x-ray regions. The measurement accuracy was investigated by varying the aperture size. This method can be expanded to a ptychographic phase retrieval method.[27,28] The recovered phase profiles in the superposition area stabilize the phase retrieval calculations and prevent the occurrence of invalid solutions. The accuracy of the recovered results is expected to be higher.

This technique can also be applied to the characterization of a focused x-ray beam with a smaller size. The determination of its wavefront profile using only one beamwaist structure is expected to be difficult owing to the difficulty of measuring the intensity profiles with a size of 1 nm. However, its determination is possible by a stitching method using a ptychographic phase retrieval method utilizing several beamwaist structures with different illumination areas selected using a small entrance aperture.

ACKNOWLEDGMENTS

This research was supported by a Grant-in-Aid for Specially Promoted Research 18002009 (2007) and the Global COE Program, Center of Excellence for Atomically Controlled Fabrication Technology (2008) from the Ministry of Education, Culture, Sports, Science, and Technology of Japan.

[1] J. H. Bruning, D. R. Herriott, J. E. Gallagher, D. P. Rosenfeld, A. D. White, and D. J. Brangaccio, Appl. Opt. **13**, 2693 (1974).
[2] U. Bonse and M. Hart, Appl. Phys. Lett. **6**, 155 (1965).
[3] A. Momose, T. Takeda, Y. Itai, and K. Hirano, Nat. Med. **2**, 473 (1996).
[4] D. Gabor, Nature (London) **161**, 777 (1948).

[5]S. Eisebitt, J. Lüning, W. F. Schlotter, M. Lörgen, O. Hellwig, W. Eberhardt, and J. Stöhr, Nature (London) **432**, 885 (2004).
[6]J. R. Fienup, Appl. Opt. **21**, 2758 (1982).
[7]Y. Nishino, J. Miao, and T. Ishikawa, Phys. Rev. B **68**, 220101(R) (2003).
[8]H. W. Babcock, Publ. Astron. Soc. Pac. **65**, 229 (1953).
[9]J. P. Gaffard and C. Boyer, Appl. Opt. **26**, 3772 (1987).
[10]L. A. Thompson, Phys. Today **47**(12), 24 (1994).
[11]H. Yumoto, H. Mimura, S. Matsuyama, S. Handa, Y. Sano, M. Yabashi, Y. Nishino, K. Tamasaku, T. Ishikawa, and K. Yamauchi, Rev. Sci. Instrum. **77**, 063712 (2006).
[12]J. Miao, P. Charalambous, J. Kirz, and D. Sayre, Nature (London) **400**, 342 (1999).
[13]Y. Nishino, Y. Takahashi, N. Imamoto, T. Ishikawa, and K. Maeshima, Phys. Rev. Lett. **102**, 018101 (2009).
[14]Y. Takahashi, Y. Nishino, R. Tsutsumi, H. Kubo, H. Furukawa, H. Mimura, S. Matsuyama, N. Zettsu, E. Matsubara, T. Ishikawa, and K. Yamauchi, Phys. Rev. B **80**, 054103 (2009).
[15]T. Kimura, S. Handa, H. Mimura, H. Yumoto, D. Yamakawa, S. Matsuyama, K. Inagaki, Y. Sano, K. Tamasaku, Y. Nishino, M. Yabashi, T. Ishikawa, and K. Yamauchi, Jpn. J. Appl. Phys. **48**, 072503 (2009).
[16]H. Mimura, S. Handa, T. Kimura, H. Yumoto, D. Yamakawa, H. Yokoyama, S. Matsuyama, K. Inagaki, K. Yamamura, Y. Sano, K. Tamasaku, Y. Nishino, M. Yabashi, T. Ishikawa, and K. Yamauchi, Nat. Phys. **6**, 122 (2010).
[17]H. Mimura, H. Yumoto, S. Handa, T. Kimura, Y. Sano, M. Yabashi, Y. Nishino, K. Tamasaku, T. Ishikawa, and K. Yamauchi, Phys. Rev. A **77**, 015812 (2008).
[18]M. Guizar-Sicairos and J. R. Fienup, Opt. Exp. **17**, 2670 (2009).
[19]C. M. Kewish, P. Thibault, M. Dierolf, O. Bunk, A. Menzel, J. Vila-Comamala, K. Jefimovs and F. Pfeiffer, Ultramicroscopy **110**, 325 (2010).
[20]A. Schropp, P. Boye, J. M. Feldkamp, R. Hoppe, J. Patommel, D. Samberg, S. Stephan, K. Giewekemeyer, R. N. Wilke, T. Salditt, J. Gulden, A. P. Mancuso, I. A. Vartanyants, E. Weckert, S. Schöder, M. Burghammer, and C. G. Schroer, Appl. Phys. Lett. **96**, 091102 (2010).
[21]G. R. Brady and J. R. Fienup, Opt. Exp. **14**, 474 (2006).
[22]J. W. Goodman, *Introduction to Fourier Optics*, 2nd ed. (McGraw-Hill, New York, 1996), Chap. 3.
[23]S. Matsuyama, H. Mimura, H. Yumoto, K. Yamamura, Y. Sano, K. Endo, Y. Mori, Y. Nishino, K. Yamasaku, T. Shikawa, M. Yabashi, and K. Yamauchi, Rev. Sci. Instrum. **76**, 083114 (2005).
[24]K. Tamasaku, Y. Tanaka, M. Yabashi, H. Yamazaki, N. Kawamura, M. Suzuki, and T. Ishikawa, Nucl. Instrum. Methods Phys. Res. A **467–468**, 686 (2001).
[25]T. Ishikawa, K. Tamasaku, M. Yabashi, S. Goto, Y. Tanaka, H. Yamazaki, K. Takeshita, H. Kimura, H. Ohashi, T. Matsushita, and T. Ohata, Proc. SPIE **4145**, 1 (2001).
[26]S. Handa, T. Kimura, H. Mimura, H. Yumoto, S. Matsuyama, Y. Sano, K. Tamasaku, Y. Nishino, M. Yabashi, T. Ishikawa, and K. Yamauchi, Nucl. Instrum. Methods. Phys. Res. A **616**, 246 (2010).
[27]H. M. L. Faulkner and J. M. Rondenburg, Phys. Rev. Lett. **93**, 023903 (2004).
[28]G. R. Brady, M. Guizar-Sicairos and J. R. Fienup, Opt. Exp. **17**, 624 (2009).